Astron. Astrophys. 344, 918–922 (1999)

ASTRONOMY AND ASTROPHYSICS

IRAS 03313+6058: an AGB star with 30 micron emission⋆

B.W. Jiang[1,2], **R. Szczerba**[2,3], **and S. Deguchi**[4]

[1] Beijing Astronomical Observatory, Chinese Academy of Sciences, Datun Rd. No.20(A), Beijing 100012, P.R. China
[2] N. Copernicus Astronomical Center, ul. Rabiańska 8, PL-87 100 Toruń, Poland
[3] Department of Physics and Astronomy, University of Calgary, Calgary, Alberta T2N 1N4, Canada
[4] Nobeyama Radio Observatory, Minamimaki, Minamisaku, Nagano 384–1305, Japan

Received 25 September 1998 / Accepted 13 January 1999

Abstract. This paper reports a detection of the 30 micron emission feature from the C–rich Asymptotic Giant Branch (AGB) star IRAS 03313+6058 based on the ISO–SWS observation. Modeling of the spectral energy distribution shows that this emission starts at about 20 micron and possibly extends to the limit (45 micron) of the observation. By assuming MgS as the carrier, the number ratio of Sulfur atoms in MgS to Hydrogen atoms in total, n(S)/n(H), is 3.0×10^{-6} as derived from model fitting. A comparison is made between this emission feature and other AGB and post–AGB objects.

Key words: stars: individual: IRAS 03313+6058 – stars: circumstellar matter – stars: chemically peculiar – stars: AGB and post-AGB

1. Introduction

The 30 micron emission was first observed in the bright AGB star, IRC+10216 (Low et al. 1973). Observations of several carbon stars by Goebel & Moseley (1985) found that the emission also occurs in AFGL 3068. Recent ISO observations of some carbon stars turned up a few more candidates: AFGL 2256, AFGL 2155 and IRC+40540 (Yamamura et al. 1998). The feature is seen not only in extreme C–rich AGB stars, but also in C–rich proto–planetary nebulae (PPNe; called also post–AGB objects) and planetary nebulae (PNe). Omont et al. (1995) observed five C–rich PPN objects with an unidentified emission feature at 21 micron in their IRAS LRS spectra (Kwok et al. 1989) and detected the 30 micron feature in all of them. In the case of PNe a similar feature is observed for IC 418 and NGC 6752 (Forrest et al. 1981). A few suggestions for the carrier of this emission have been proposed. Because the feature has never been detected in O–rich objects, and is the broadest known feature in the mid–infrared, solid species that form in the absence of oxides are taken into consideration. Omont et al. (1995) suggested iron atoms bound to PAH molecules as a possible emitter for the 30 micron feature. But Chan et al. (1997) raise doubt about this suggestion after the detection of this feature in direction of the Galactic center, where the existence of PAH molecules is questionable. A more acceptable candidate is solid magnesium sulfide (MgS), first suggested by Goebel & Moseley (1985). The laboratory spectra of MgS samples showed very good agreement of band turn–on and cut–off wavelengths, as well as the overall band shape, with the observed feature seen in AFGL 3068 and IRC+10216. A reasonable fit was achieved to the 30 micron feature of the PPN object IRAS 22272+5435 (Szczerba et al. 1997) by means of MgS grains with a distribution of shapes. In addition, MgS is one of the molecules which condensate at low temperature when no oxides are present. This is consistent with the detection of the 30 micron feature only in objects with cold dust shells.

IRAS 03313+6058 was classified as a candidate extreme carbon star based on the similarity of its IRAS LRS spectrum to those of AFGL 3068 and IRC+10216 (Volk et al. 1992). It has no optical counterpart in the POSS plates (Jiang & Hu 1992). In the near infrared, the source was detected at K=15.6 mag and was not detected in the J and H bands with upper limits of magnitude 17 and 16, respectively (Jiang et al. 1997). The color index between 12 and 25 micron, based on the IRAS PSC catalogue, indicates a color temperature of about 250 K. Therefore, this is an object with a cold and optically thick circumstellar envelope. Though the IRAS LRS type of this object is 22, no clear silicate feature is seen (note that Kwok et al. 1997 classified the LRS spectrum of this object as unusual). The detection of HCN (1–0) line (Omont et al. 1993) indicated the possibility of a C–rich nature. O–rich maser lines such as OH (Le Squeren et al. 1992, Galt et al. 1989), H_2O (Wouterloot et al. 1993) or SiO (Jiang et al. 1996) have not been detected at all and this is an indirect indication of a C–rich circumstellar envelope. The CO (2–1) line profile suggests that this object is a late–type star rather than a young stellar object, and gives an expansion velocity of the shell of 13.9 km s^{-1} (Volk et al. 1993).

2. Observation and data reduction

The spectroscopic observation was carried out by using the SWS spectrometer (de Graauw et al. 1996) of the Infrared Space Ob-

Send offprint requests to: Biwei Jiang (jiang@class1.bao.ac.cn)

⋆ Based on observations with ISO, an ESA project with instruments funded by ESA Member States (especially the PI countries: France, Germany, the Netherlands and the United Kingdom) and with participation of ISAS and NASA

servatory (ISO) satellite on 31 July 1997 with the fastest scan speed covering full wavelength range from 2.3 μm to 45 μm (AOT 01, speed 1). The achieved resolution is about 200 $\sim$ 300 with S/N higher than 100 at wavelength longer than 5 μm.

The original pipeline data were corrected for dark current, up–down scan difference, flat–field and flux calibration by using the SWS Interactive Analysis (IA) at MPE Garching[1]. The deglitching and averaging to equidistant spectral point in wavelength across the scans and detectors was done using the ISAP package.

The ISOCAM imaging was performed on 31 July 1997 with the CAM camera in the mode AOT 01 with the filter LW3, centered at 15 micron. The data were reduced by using CIA (a joint development by the ESA Astrophysics Division and the ISOCAM Consortium led by the ISOCAM PI, C. Cesarsky, Direction des Sciences de la Matiere, C.E.A., France; Cesarsky et al. 1996). The object is still point-like at this angular resolution of 1.5 arcsec/pixel. The flux through the filter LW3 is 59.03 Jy as measured by aperture photometry method, about twice of the 12 μm flux (30.87 Jy) given by the IRAS PSC catalogue. This difference could be caused by the strong emission in the mid–infrared range of the spectrum or by the object being variable. However, the flux ($\sim$ 39 Jy) at 15 micron of the SWS spectrum, which was taken at the same day as the ISOCAM image, does not match the photometric result from the ISOCAM image while it is in rough agreement with the 12 μm IRAS flux. By calculating the IRAS fluxes at 12 and 25 micron from SWS, correction factors of 1.11 and 1.06 should be applied to the corresponding SWS bands, respectively, to agree with the photometric data from IRAS PSC. After correction, the spectrum is smooth and the shape is similar to its IRAS LRS spectrum. In the same time, the IRAS LRS spectrum should be multiplied by a factor of 1.27 to agree with the IRAS PSC data. These factors are within the calibration uncertainties of the ISO–SWS and the IRAS LRS. Such agreement may show that the flux calibration of ISO–SWS is reliable, and that the object is non–variable (the variability index from IRAS observation is 50, at the border between variable and nonvariable indices). Therefore, we suspect that the discrepancy between ISO–SWS and ISO–CAM results is related to the uncertainties in the flux calibration from the image at LW3 band, but the reason for this is not clear to us. Anyway this ISO-CAM result is shown in Fig. 1 as an open circle.

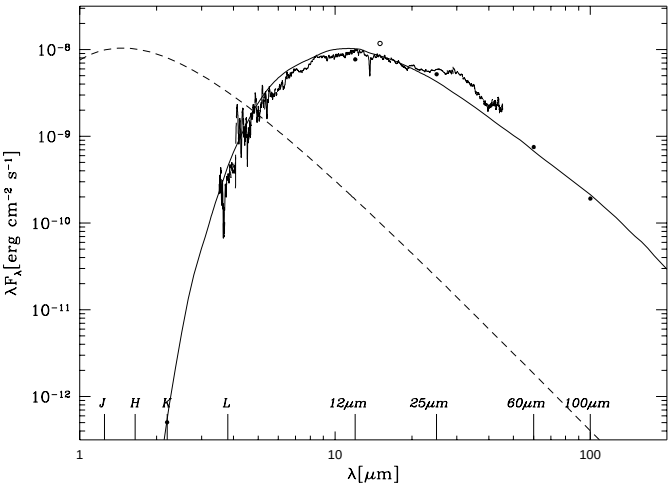

Fig. 1. Observed and modelled spectral energy distribution. The dot represents the near infrared and IRAS photometric results and the thin solid line is the ISO–SWS spectrum starting from band 1E. The flux at 15 micron measured from the ISO–CAM LW3 image is given by an open circle. The thick line is calculated from the model with the values of the parameters listed in Table 1 and the long–dashed line represents the radiation spectrum from the central star which radiates as a blackbody of temperature 2500 K.

3. Modeling

3.1. Spectral energy distribution

The overall spectral energy distribution of this object is observationally determined from the near infrared to the far infrared. The K band magnitude at 2.2 micron is 15.6 (Jiang et al. 1997), i.e., the flux is 3.7×10^{-4} Jy. The fluxes at 12, 25, 60 and 100 μm are 30.87, 43.44, 15.08 and 6.40 Jy, respectively, from the IRAS photometric observations (quality index = 3 in all four IRAS bands). Combination of these photometric results with the ISO SWS 01 spectrum defines the observed spectral energy distribution. In Fig. 1, the observational data are shown where the dots represent the photometric results and the thin solid line shows the ISO SWS 01 spectrum. The spectrum of ISO–SWS from 2.3 micron to 3.52 micron (band 1A, 1B and 1D of ISO–SWS) is not shown because it is too noisy.

The model we used to fit the observational data is described in detail by Szczerba et al. (1997). In brief, the frequency–dependent radiative transfer equations are solved under the assumption of spherically–symmetric geometry simultaneously with the thermal balance equation for a dusty envelope. The radiation of the central star is assumed to be of a blackbody. The mass loss rate is taken to be constant and the envelope is assumed to expand at the velocity derived from the CO (2–1) line observation. The dust opacity is represented by amorphous carbon grains of AC type (Bussoletti et al. 1987, Rouleau & Martin 1991).

The appropriate values of important parameters for fitting the observational data are listed in Table 1. The symbols have their usual meanings, but more details can be found in Szczerba et al. (1997). Dynamical time t_{dyn} means the time required for the matter to reach the outer radius of the envelope.

The result from model calculation with the values listed in Table 1 is plotted in Fig. 1 by a heavy solid line, while the long–dashed line represents the radiation from the central star, which radiates as a blackbody of effective temperature 2500 K. The luminosity and distance of the star depend on each other, as well as the dust–to–gas mass ratio and mass loss rate assumed. We adopted the value of 8000 $L_\odot$ for the luminosity. The corresponding distance is 4.25 kpc. Since the outer radius R_{out} is 7.0

[1] We acknowledge support from the ISO Spectrometer Data Centre at MPE Garching, funded by DARA under grant 50 QI 9402 3

Table 1. Model parameters

parameter	value
T_{eff}	2500 K
L_{star}	8000 $L_\odot$
d	4.25 kpc
T_{inner}	760 K
R_{inner}	5.8×10^{14} cm
R_{out}	7.0×10^{17} cm
$\dot{M}$	8.0×10^{-5} $M_\odot$/yr
t_{dyn}	1.6×10^{4} yr
Dust–to–gas ratio	5.0×10^{-3}
a_-	0.005 μm
a_+	0.25 μm
p (power–law index of size dist.)	3.5

$\times$ 10^{17} cm, the angular diameter of the circumstellar envelope is predicted to be 22 arcseconds at this distance. This size is big enough to be resolved by the ISOCAM at the resolution mode of 1.5″. However, the ISOCAM observations centered at 15 μm are the most sensitive for the peak temperature of about 200 K which, according to modeling results, corresponds to radius of 4.1×10^{15} cm and reflects a much smaller angular size of about 0.13 arcseconds. So the result of ISOCAM that no extension is seen may be attributed to a large distance of the object. The value of R_{out} is determined from the model–fitting to the observational results and its choice affects mainly the flux intensity in the mid– and far–infrared. A reasoanable fit can be achieved with R_{out} values ranging from 5.0×10^{17} cm to 9.0×10^{17} cm assuming a constant mass loss rate. For increasing mass loss rate (which means density distribution steeper than r^{-2}), the outer radius should be larger to compensate for the smaller far-infrared emission of the outer envelope layers, but the range of the allowed changes in R_{out} is quite similar. Note, however, that such a density distribution cannot be much different from that corresponding to the constant mass loss rate due to strong constraints from the 60 and 100 μm flux densities unless we assume that the dust optical properties at far infrared wavelengths have a less steep slope than in the case of amorphous carbon used here.

The adopted dust–to–gas mass ratio of $5.0\times$ 10^{-3} corresponds to mass loss rate of 8.0×10^{-5} $M_\odot$/yr. This mass loss rate is higher than 5.8×10^{-6} $M_\odot$/yr deduced from CO (1–0) line (Loup et al. 1993) or 1.4×10^{-5} $M_\odot$/yr inferred from CO (2–1) line (Omont et al. 1993). Note, in addition, that to get velocity of the shell around 14 km s^{-1} dynamical considerations would suggest even smaller value of dust–to–gas mass ratio (see Steffen et al. 1998), and in consequence a larger mass loss rate and a larger total mass of the envelope. However, the assumption of a density distribution slightly steeper than r^{-2} would cancel the increase in total mass of the envelope. The calculation of the mass loss rate from the CO line suffers mainly from the uncertainty of the distance and mass fraction factor for CO molecules. For example, the mass loss rate of W Hya derived from infrared water lines lies a factor about 30 above the estimates based on the CO line observation (Neufeld et al. 1996). The case of Y CVn is similar in that the mass loss rate derived from interpretation of far infrared ISOPHOT images is 2 orders of magnitude higher than that found from the CO line (Izumiura et al. 1996). Izumiura et al. (1996) explained the result for Y CVn by suggesting that the far infrared and CO observations represent different epoches of mass loss. There may be another possibility that, the mass fraction of CO molecules is overestimated so that the mass loss rate is underestimated. The mass loss rate of IRAS 03313+6058 from modeling lies a little above that estimated from the flux at 60 micron, 4.8×10^{-5} $M_\odot$/yr (Omont et al. 1993). The derivation of the mass loss rate from the flux at IRAS bands depends on the distance and on the bolometric correction factor which would introduce some uncertainty. Though the mass loss rate derived from our modeling depends on the value of dust–to–gas ratio and density distribution, the result is relatively stable (probably better than a factor of two) because of the constraints required to fit the spectral energy distribution over the wide–range of wavelengths. The object then experiences quite strong wind, and has a circumstellar envelope perhaps as massive as 1.282 $M_\odot$. By considering that the outer radius R_{out} can vary in the range from 5.0×10^{17} to 9.0×10^{17} cm, the mass of the circumstellar envelope may be in the range of 0.92 $M_\odot$ to 1.65 $M_\odot$ under the assumed dust–to–gas ratio of 0.005. Since the mass of the cirsumstellar envelope appears to be above one solar mass, the star could very possibly be an intermediate–mass AGB star.

3.2. The 30 micron emission

As can be seen in Fig. 1, the object shows emission around 30 micron which is superimposed on the continuum radiation from the star and the circumstellar envelope. The emission starts at 20 micron, peaks at about 30 micron and extends to longward of 40 micron. Because of another unidentified emission around 43.6 micron (see Discussion), it is difficult to define the cut–off position of the 30 micron emission band from this spectrum, though the emission may extend to the long–wavelength limit of ISO–SWS.

As described in the Introduction, MgS is regarded as a reasonable candidate to be the carrier of the 30 micron emission. We tried to model this with optical constants taken from the tables based on laboratory measurements of a MgS(90%)–FeS(10%) mixture (Begemann et al. 1994). For our computations, we used two shapes for the grains, i.e. the CDE (Continuous Distribution of Ellipsoids) and Mie theory (spherical grains). Assumptions and method used are described in detail by Szczerba et al. (1997).

Because the temperature structure of the circumstellar envelope is determined from modeling of the spectral energy distribution, and because there is little difference in the dust temperature structure between the largest and smallest AC grains (a_- = 0.005 and a_+ = 0.25 μm) used in the calculations, the only free parameter after taking MgS into account is the number ratio between the Sulfur atoms in MgS and the total number of Hydrogen atoms n(S)/n(H). Under the CDE approximation a value

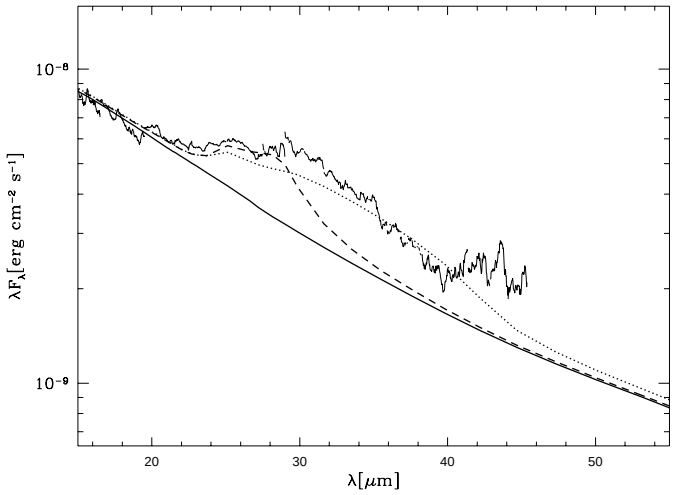

Fig. 2. Fitting the 30 micron emission. The thin solid line is the ISO–SWS spectrum and the thick line stands for the model fitting result to spectral energy distribution, the same as in Fig. 1. The dotted and dashed lines represent the fitting by assuming the CDE and Mie approximations for the computation of optical properties of the MgS grains, respectively; n(S)/n(H) = 3.0×10^{-6}.

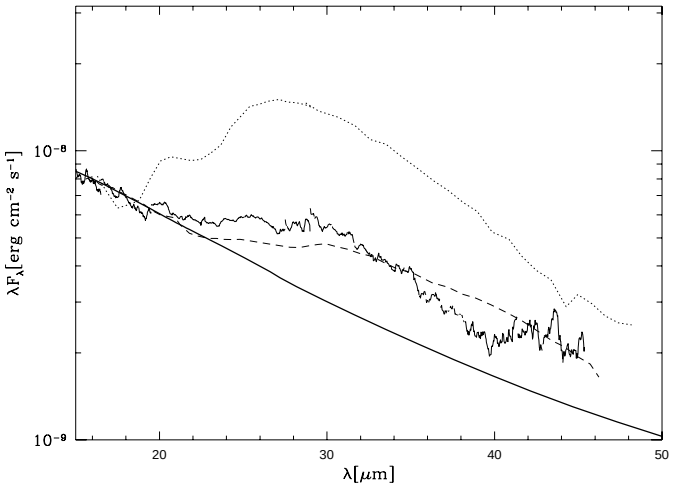

Fig. 3. Comparison of the 30 micron band in IRAS 03313+6058 (thin solid line) with the post–AGB object IRAS 22272+5435 (dotted line) and AGB star AFGL 3068 (dashed line). The modeling continuum spectrum at this band to IRAS 03313+6058 is represented by the thick solid line which lies below the emission features.

of 3.0×10^{-6} for n(S)/n(H) gives a fit to the observed feature at the long–wavelength wing, though there is a little inadequacy in the short–wavelength wing of the band. On the other hand, the Mie theory (spherical) grains can make up the emission at the short–wavelength wing. This means that a combination of MgS grains shapes may account for the observed emission. In Fig. 2, the observation and modeling of this band are shown.

4. Discussion

It is interesting to compare the 30 micron feature of this object with those of other AGB and post–AGB stars. Fig. 3 exhibits the spectrum of IRAS 03313+6058 together with the profiles of this feature for another AGB star, AFGL 3068, and for the post–AGB object IRAS 22272+5435. The data for AFGL 3068 are taken from Yamamura et al. (1998) while the data for the IRAS 22272+5435 are from Omont et al. (1995). Because these two objects are much brighter than IRAS 03313+6058, their spectra are scaled downward to agree at about 20 μm with the spectrum of IRAS 03313+6058. Besides that IRAS 22272+5435 has another feature at 21 micron, the most evident difference is that the emission of IRAS 03313+6058 is much weaker than that of IRAS 22272+5435. On the other hand, AFGL 3068 exhibits a similar strength of the 30 μm band as does IRAS 03313+6058 which seems, however, to show more fine structures in this wavelength range.

The 30 micron emission for IRAS 22272+5435 was previously modeled using MgS grains (Szczerba et al. 1997). That fit resulted in an estimate of n(S)/n(H) = 4×10^{-6} for the highest dust temperature distribution and 1.6×10^{-5} for the lowest dust temperature distribution considered. The value of 3.0×10^{-6} for IRAS 03313+6058 is very close to the case of highest dust temperature distribution of IRAS 22272+5435. Then there is probably little difference in the sulfur abundance between these two objects and the strength of the 30 micron emission band may be influenced more strongly by other factors. The temperature may be one of the important factors through the way that lower temperature favors the excitation of this band. As the dust temperature of post–AGB envelopes is generally lower than that of AGB ones, this emission is stronger in post–AGB stars. For example IRAS 22272+5425 has colder dust than IRAS 03313+6058 and much stronger emission at this band. From laboratory experiment, MgS is one of the molecules which condenses at low temperature in the environment without oxides. Up to now, this band emission is detected in the C–rich AGB stars only with cold and high optical depth dust shells. This may indicate the existence of a critical temperature to form the 30 micron emission band carrier, and that such low temperatures together with approporiate chemical conditions are only possible in the extreme carbon stars. On the other hand, it is still not clear if carbon stars with smaller mass loss rates could form a carrier of this band. The existence of the 30 μm emission in AFGL 2155 and IRC+40540 (Yamamura et al. 1998), neither was classified as extreme C–stars by Volk et al. (1992), suggests that formation of the approporiate chemical material is much more common and that higher envelope temperature in other carbon stars (not extreme ones) does not allow us to detect this emission feature. But it could be as well that some special chemical reactions responsible for the carrier formation of the 30 μm band are efficient only when temperature is enough low and/or the chemical composition is approporiate. Unfortunately, since without optical spectra the determination of the chemical abundances is rather impossible other methods of investigation should be elaborated, and especially better statistics created by the ISO data could help solve the problem of the 30 μm carrier formation.

Besides this feature around 30 micron, some other features, e.g. absorptions around 7.5 and 14 micron, emissions around 41 and 43.5 μm in the SWS spectrum of this object are not discussed here; they are currently under investigation. We note only that the absorptions are probably related to the C_2H_2 and/or HCN molecular bands, while emissions could be related to the crystaline silicates (especially as the enstatite mass absorption coefficient matches these emissions well - see Jäger et al. 1998). If crystalline silicate emissions are confirmed then it will allow to deduce an evolutionary status of IRAS 03313+6058 which could bring some more information on the exciting transition phase between oxygen and carbon rich parts of the AGB evolution.

Acknowledgements. B.W.J. thanks the people in N. Copernicus Astronomical Center, Torun for their help and support. We express also our gratitudes to Dr. Kevin Volk for his careful reading of the manuscript and useful suggestions. This work has been partly supported by grant 2.P03D.002.13 of the Polish State Committee for Scientific Research.

References

Begemann B., Dorschner J., Henning T., Mutschke H., Thamm E., 1994, ApJ 423, L71
Bussoletti E., Colangeli L., Borghesi A., Orofino V., 1987, A&AS 70, 257
Cesarsky C.J., Abergel A., Agnese P., et al., 1996, A&A 315, L32
Chan K.W., Moseley S., Casey S., et al., 1997, ApJ 483, 798
de Graauw Th., Haser L., Beintema D., et al., 1996, A&A 315, L345
Forrest W.J., Houck J.R., McCarthy J.F., 1981, ApJ 248, 195
Galt J., Sun K., Frankow J., 1989, AJ 98, 2182
Goebel J., Moseley S., 1985, ApJ 290, L35
Izumiura H., Hashimoto O., Kawara K., Yamamura I., Waters L.B.F.M., 1996, A&A 315, L221
Jäger C., Molster F.J., Dorschner J., et al., 1998, A&A 339, 904
Jiang B.W., Hu J.Y., 1992, ChA&A 16, 416
Jiang B.W., Deguchi S., Yamamura I., et al., 1996, ApJS 106, 463
Jiang B.W., Deguchi S., Hu J.Y., et al., 1997, AJ 113, 1315
Kwok S., Volk K., Hrivnak B.J., 1989, ApJ 345, L51
Kwok S., Volk K., Bidelman W.P., 1997, ApJS 112, 557
Le Squeren A.M., Sivagnanam P., Dennefeld M., David P., 1992, A&A 254, 133
Loup C., Forveille T., Omont A., Paul J.F., 1993, A&AS 99, 291
Low F., Rieke G., Armstrong K., 1973, ApJ 183, L105
Neufeld D., Chen W., Melnick G., et al., 1996, A&A 315, L237
Omont A., Loup C., Forveille T., et al., 1993, A&A 267, 515
Omont A., Moseley S., Cox P., et al., 1995, ApJ 454, 819
Rouleau F., Martin P.G., 1991, ApJ 377, 526
Steffen M., Szczerba R., Schönberner D., 1998, A&A 337, 149
Szczerba R., Omont A., Volk K., Cox P., Kwok S., 1997, A&A 317, 859
Volk K., Kwok S., Langill P., 1992, ApJ 391, 285
Volk K., Kwok S., Woodsworth A., 1993, ApJ 402, 292
Wouterloot J., Brand J., Fiegle K., 1993, A&AS 98, 589
Yamamura I., de Jong T., Justtanont K., Cami J., Waters L.B.F.M., 1998, Ap&SS 255, 351